Joule

CellPress

Article

A Single-Junction Cathodic Approach for Stable Unassisted Solar Water Splitting

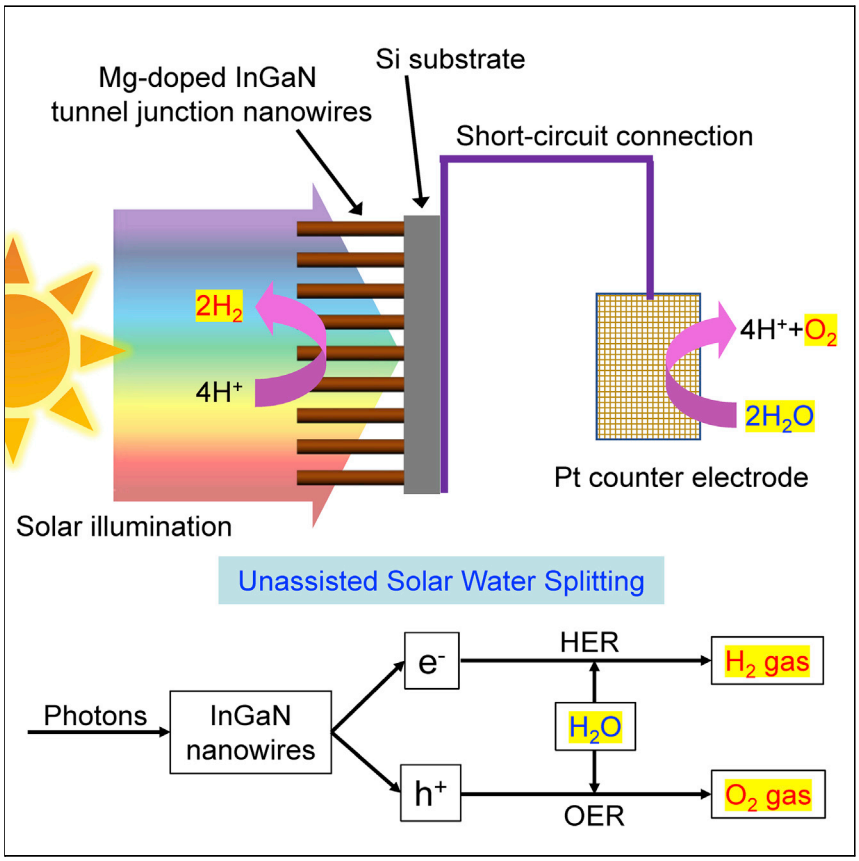

A single-junction InGaN nanowire photocathode monolithically integrated on silicon wafer was demonstrated to drive relatively efficient and stable solar water splitting. A solar-to-hydrogen (STH) conversion efficiency of 3.4% was measured at zero bias in two-electrode configuration under AM1.5G one-sun illumination. The InGaN nanowire photocathode can operate efficiently for ~300 h of unassisted solar water splitting without using extra surface protection.

Yongjie Wang, Yuanpeng Wu, Jonathan Schwartz, Suk Hyun Sung, Robert Hovden, Zetian Mi

ztmi@umich.edu

HIGHLIGHTS

Unassisted solar water splitting is demonstrated on InGaN nanowire photocathodes

An STH efficiency of 3.4% is reported for single-junction semiconductor photoelectrodes

Long-term stability of 300 h is demonstrated without extra passivation layers

Wang et al., Joule 3, 2444–2456
October 16, 2019
https://doi.org/10.1016/j.joule.2019.07.022

Joule

CellPress

Article

A Single-Junction Cathodic Approach for Stable Unassisted Solar Water Splitting

Yongjie Wang,[1] Yuanpeng Wu,[1] Jonathan Schwartz,[2] Suk Hyun Sung,[2] Robert Hovden,[2] and Zetian Mi[1,3,*]

SUMMARY

Unassisted solar water splitting is one key step of artificial photosynthesis converting solar energy to chemical fuels. To date, however, there has been no demonstration of efficient and stable semiconductor photoelectrodes without extra surface protection for unassisted solar water splitting. In this work, we show that a single-junction approach of p-type $In_{0.25}Ga_{0.75}N$ nanowires monolithically integrated on n-type Si wafers through an n^{++}/p^{++}-InGaN tunnel junction can drive relatively efficient and stable unassisted water splitting. A photocurrent density of 2.8 mA cm^{-2} was measured at zero bias versus a platinum counter electrode in a two-electrode configuration, leading to a solar-to-hydrogen efficiency of 3.4%. No performance degradation was observed for ~300 h of unassisted solar water splitting without using any extra surface protection layers. Such a single-junction photocathode can be further integrated with a narrow band-gap junction, e.g., Si or GaAs, to achieve further improved efficiency for long-term stable solar water splitting.

INTRODUCTION

In the past decades, photoelectrochemical water splitting, which has been considered one of the most promising approaches to convert solar energy directly to chemical fuels, has been intensively studied.[1–3] To date, however, there has been no demonstration of a highly efficient and stable photoelectrochemical device using semiconductor photoelectrodes without extra surface protection for unassisted solar water splitting.[4–10] Illustrated in Figure 1 are the schematic energy band diagrams of semiconductor photoelectrodes representing three commonly used approaches to achieve unassisted photoelectrochemical solar water splitting,[1] including the use of single-junction,[1,5] double-junction,[11,12] and multiple-junction semiconductor structures,[13] which have also been referred to as single-photon, two-photon, and multi-photon approaches, respectively.[11,14] Conventional single-junction semiconductor photoelectrodes often do not meet the stringent band edge positions and thermodynamic overpotentials required for photoelectrochemical water splitting[4] and, consequently, cannot drive unbiased water splitting under visible light.[15–18] Therefore, double- or multi-junction structures, i.e., the so-called Z-scheme, have been proposed and intensively studied to achieve unassisted solar water splitting.[12,14,19] A theoretical solar-to-hydrogen conversion efficiency of ~27% has been predicted for a double-junction photoelectrode consisting of a 1.70 eV top junction and a 1.05 eV bottom junction under AM1.5G one-sun illumination.[20] While Si, given its narrow energy band gap (~1.1 eV), scalable manufacturing, and mature fabrication process, is ideally suited for the bottom light absorber, it has remained extremely challenging to identify a practical top light absorber that is stable in photoelectrochemical reaction and can be monolithically integrated with Si. As such,

Context & Scale

Hydrogen gas, as an alternative to fossil fuels, is an important clean energy source without emitting any greenhouse gas, which can be produced from solar water splitting through the dissociation of water molecules to H_2 and O_2 gases under solar illumination. To date, however, there have been no such solar water-splitting systems for efficient and stable hydrogen production. In this work, we demonstrate a single-junction cathodic approach for solar hydrogen production. p-Type $In_{0.25}Ga_{0.75}N$ nanowires monolithically integrated on n-type silicon wafers through an n^{++}/p^{++}-InGaN tunnel junction can drive relatively efficient and stable unassisted water splitting under simulated solar illumination. Beyond this demonstration, such single-junction InGaN nanowire structures can be integrated with Si or GaAs bottom light absorbers forming double-junction photoelectrodes, which can potentially lead to much higher efficiency with long-term stable operation.

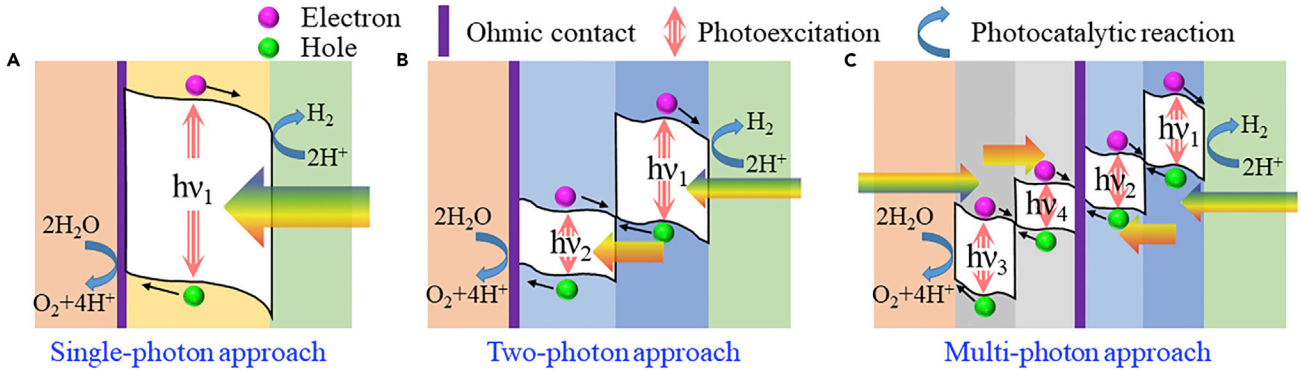

Figure 1. Schematic Illustration of the Energy Band Diagrams of Semiconductor Photoelectrodes for Unassisted Solar Water Splitting

(A) Single-photon approach driven by a single-junction semiconductor.

(B) Two-photon approach using the Z-scheme tandem structures.

(C) Multi-photon approach by integrating multiple semiconductor junctions.

there have been only few demonstrations of double-junction photoelectrodes, e.g., $GaInP_2$/GaAs and WO_3/$BiVO_4$,[6–8,10] that can drive unbiased solar water splitting.

It is therefore highly desirable to develop a semiconductor photoelectrode that can operate efficiently and stably under visible light and can be directly integrated onto Si wafers. Recently, III-nitride semiconductor nanostructures, e.g., InGaN, have shown extraordinary potential for direct solar water splitting.[21–24] By varying the alloy compositions, their energy band gaps can be continuously tuned from ultraviolet, through visible, to the near-infrared.[25] Significantly, the energy band edge positions of InGaN can straddle water redox potentials for indium compositions up to 40%–50%, which corresponds to an energy band gap of ~1.7 eV.[25] In spite of these promises, however, the realization of a single-junction InGaN photoelectrode that can drive photoelectrochemical solar water splitting stably and efficiently without any external bias has remained elusive.[21,22,26,27] The underlying challenges include the corrosion and oxidation of the exposed Ga or In atoms, which, together with the presence of surface states and defects, lead to surface recombination and material degradation during harsh photocatalytic reaction. In addition, conventional InGaN materials grown on Si generally exhibit very large densities of defects and dislocations,[28–30] which makes it difficult for the efficient collection of photo-generated holes through the underlying Si wafer while simultaneously achieving efficient extraction of photo-generated electrons at the InGaN/electrolyte interface.

To overcome these challenges, we have investigated a single-junction InGaN nanowire photocathode epitaxially grown on Si wafer using plasma-assisted molecular beam epitaxy. The use of a nanowire tunnel junction enables the direct integration of p-InGaN nanowire arrays on n-type Si wafer with fewer dislocations due to the surface strain relaxation. Efficient charge carrier separation is facilitated by optimizing the surface band bending of InGaN nanowires through controlled p-type (Mg) dopant incorporation.[31,32] Photo-generated electrons can readily migrate to the lateral surfaces of nanowires to drive proton reduction due to the downward band bending, whereas photo-generated holes are collected by the underlying Si wafer through the tunnel junction incorporated in each nanowire. With the use of plasma-assisted epitaxy, the surface of such nanostructures can be engineered to be N rich, which can protect against photo-corrosion and oxidation in harsh photocatalytic reaction.[33,34]

[1]Department of Electrical Engineering and Computer Science, University of Michigan, 1301 Beal Avenue, Ann Arbor, MI 48109, USA

[2]Department of Materials Science and Engineering, University of Michigan, 2300 Hayward Street, Ann Arbor, MI 48109, USA

[3]Lead Contact

*Correspondence: ztmi@umich.edu

https://doi.org/10.1016/j.joule.2019.07.022

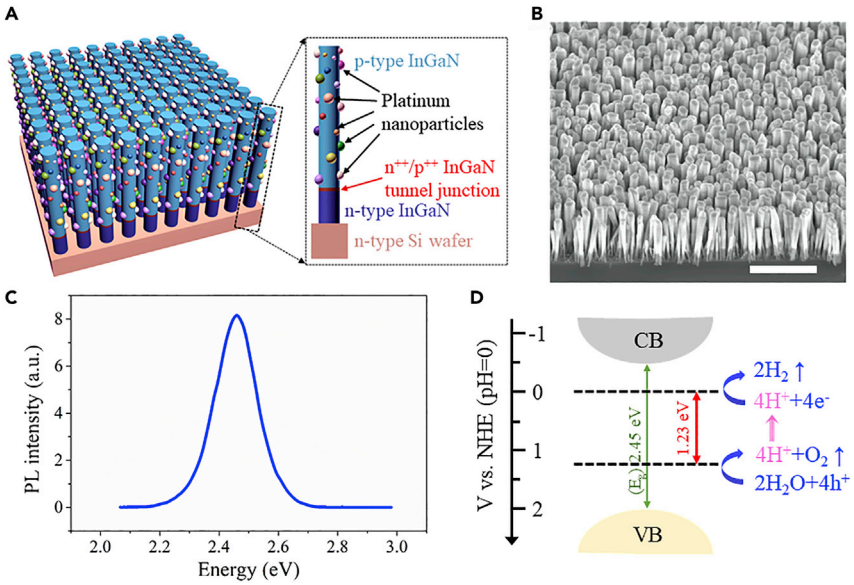

Figure 2. Design and Properties of $In_{0.25}Ga_{0.75}N$ Nanowires for Unassisted Solar Water Splitting

(A) Schematic illustration of InGaN nanowire tunnel-junction structure grown directly on planar n-type Si wafer. Each nanowire includes an n-InGaN, n^{++}/p^{++}-InGaN tunnel junction, and p-InGaN segment. Pt co-catalyst nanoparticles were also deposited on the nanowire surface.

(B) Secondary electron SEM image of InGaN nanowire tunnel-junction structures grown on planar Si surface. Scale bar, 1 μm.

(C) Room-temperature photoluminescence spectrum of InGaN nanowires with an energy gap of ~2.45 eV, corresponding to an indium composition of ~25%.

(D) Schematic illustration of band edge positions of $In_{0.25}Ga_{0.75}N$ nanowires straddling water redox reaction potentials.

Here, we have demonstrated that an $In_{0.25}Ga_{0.75}N$ nanowire photocathode grown directly on Si wafer can exhibit relatively efficient and stable unassisted solar water splitting. At zero bias versus Pt counter electrode, an InGaN nanowire photocathode can exhibit an STH efficiency of 3.4%, which, to the best of our knowledge, is the highest efficiency value ever achieved in a single-photon system for unbiased photoelectrochemical water splitting. Significantly, stable operation for ~300 h has been demonstrated in two-electrode measurement under AM1.5G one-sun illumination. With further optimization of the nanowire sizes, compositions, doping, and energy band gap, and the monolithic integration with a bottom Si, or GaAs light absorber, it may be possible to achieve the Z-scheme structure with a potential STH efficiency of over 20%.[1,7,11,35]

RESULTS

Design and Synthesis of Single-Junction InGaN Nanowire Photocathode

Schematically illustrated in Figure 2A is an InGaN nanowire photocathode, grown on a commercial Si wafer using plasma-assisted molecular beam epitaxy (see Experimental Procedures). In this simplified diagram, each nanowire consists of an n-type (Ge-doped) InGaN segment, n^{++}/p^{++}-InGaN tunnel junction, and p-type (Mg-doped) InGaN segment. The top p-InGaN serves as the light absorber. The use of n^{++}/p^{++}-InGaN tunnel junction can significantly reduce the resistivity between p-InGaN nanowires and the underlying n-Si wafer, demonstrated in Figure S1.[28,36,37] Linear sweep voltammetry (LSV) measurement of p-type InGaN nanowires directly grown on heavily doped Si substrate without using tunnel-junction structure shows a much worse fill factor due to the large resistivity between Si

substrate and p-InGaN materials, which can be further confirmed from the impedance measurement (Figure S1B). Significantly, InGaN tunnel junction also enhances the separation of photo-generated electrons and holes. Under light illumination, photo-generated holes in p-InGaN migrate toward the p^{++}-InGaN tunnel-junction layer and efficiently recombine with electrons in n^{++}-InGaN tunnel-junction layer supplied from Si substrate. The net effect is that photo-generated holes in the p-InGaN segment migrate toward the photoanode through the tunnel junction and Si substrate. Moreover, the semiconductor/electrolyte junction prevents electrons in n-InGaN material and holes in p-InGaN material to leak into the electrolyte solution due to the surface band bending, which further ensures that such tunnel-junction structure functions well without shorting issues in conductive electrolyte solution. Platinum nanoparticles were photo-deposited on InGaN nanowire surfaces (see Experimental Procedures), which provide kinetically catalytic sites for efficient water reduction reaction.[38–40] Shown in Figure 2B is the scanning electron microscopy (SEM) image of InGaN tunnel-junction nanowires, which have lengths of ~886 (±123) nm and diameters of ~112 (±36) nm. Such relatively small-diameter nanowire geometry was adopted to reduce charge transfer distance to catalytic sites of photo-generated electrons in the p-InGaN segment, which is often a bottleneck for conventional planar photoelectrodes.[31,41,42] Shown in Figure 2C is the photoluminescence (PL) spectrum of such InGaN nanowires measured at room temperature (see Experimental Procedures). The PL emission wavelength is ~506 nm, corresponding to an energy gap of ~2.45 eV and an indium composition of ~25%. The relatively small full-width at half-maximum (FWHM) of ~0.16 eV suggests good crystalline quality of InGaN nanowires.[37,43,44] Illustrated in Figure 2D, the conduction band (CB) and valence band (VB) edges of $In_{0.25}Ga_{0.75}N$ can straddle the water redox potentials with relatively large overpotentials for water splitting, which is usually a limiting factor for other single-junction semiconductors to achieve unassisted solar water splitting.[22,25,45,46]

Structural Characterization of InGaN Nanowires

High-resolution electron microscopy of the InGaN nanowires confirms many of the key features illustrated in Figure 2A—vertically continuous InGaN domains within highly crystalline nanowires grown across a Si substrate with Pt nanoparticles dispersed onto the surfaces; however, the actual structure deviates in uniformity, morphology, and chemical homogeneity from an ideal structure. Elemental mapping by energy dispersive X-ray (EDX) performed from the top side of InGaN nanowires (Figures 3A and 3B) confirms a continuous distribution of molecular beam epitaxy (MBE)-grown InGaN nanowires across the Si wafer. The structural details within the nanowire array are revealed in cross-sectional, high-angle, annular dark-field scanning transmission electron microscopy (HAADF-STEM) (Figure 3C). The wires have a typical length of ~886 (±123) nm and a diameter that grows from an initial size of ~30 (±7) nm to ~112 (±36) nm at the top of the wire. As such, InGaN nanowires tend to become larger in diameter along with the growth direction, especially after ~180 nm height, and may touch the adjacent nanowires due to the increased diameter and reduced interwire spacing.

Atomic resolution images reveal a highly crystalline order that extends throughout the entirety of each nanowire and to a highly faceted surface (Figures 3F and 3G). Figure 3F demonstrates the atomic crystal structure of InGaN nanowires, corresponding to InGaN (0002) wurtzite lattice plane, which also confirms the <0001> growth direction of InGaN nanowires (Figures S2 and S3).[22] The periodic ordering of atoms further demonstrates its high-quality single-crystal structure of InGaN nanowires without significant dislocations. The flat top plane suggests an N-polar

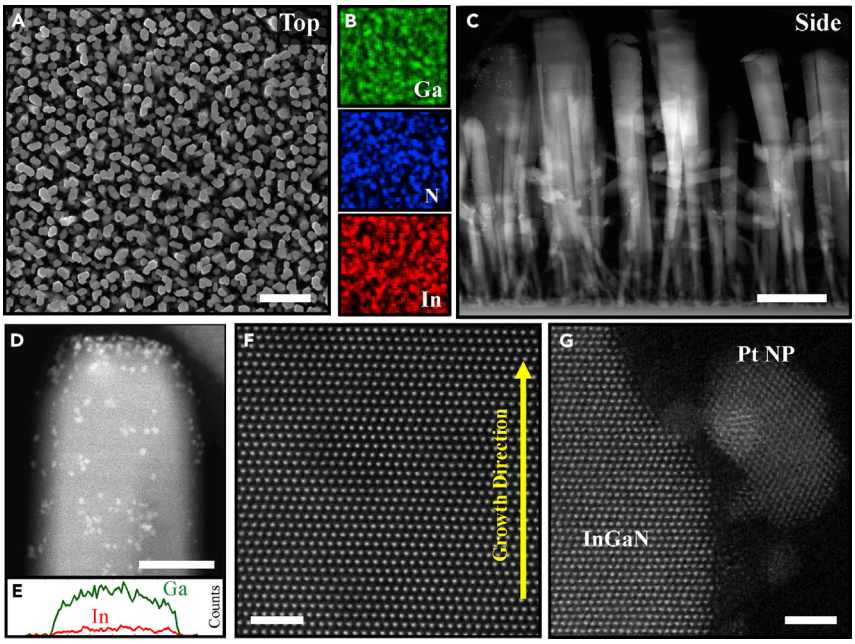

Figure 3. Electron Microscope Characterizations of MBE-Grown InGaN Nanowires with Small-Size Pt Co-catalyst Nanoparticles

(A and B) Top-view secondary electron SEM image (A) with SEM-EDX maps showing Ga, In, and N presence (B). Scale bar, 200 nm.

(C) Side-view, cross-sectional HAADF-STEM image of the InGaN nanowires. Scale bar, 200 nm.

(D) Pt nanoparticles decorated InGaN nanowire surfaces, showing the dispersed deposition of Pt co-catalyst. Scale bar, 50 nm.

(E) Ga and In concentration measured by EDX across the top section of a nanowire (acquired from similar nanowire shown in Figure S4B).

(F) Atomic resolution HAADF-STEM images reveal highly crystalline InGaN nanostructure preserved across the wire. Scale bar, 2 nm.

(G) Highly crystalline Pt nanoparticles deposited on InGaN nanowire surface. Scale bar, 2 nm.

surface of InGaN nanowires expected from growth in an N-rich MBE environment, which is more stable in chemical solution for solar water splitting.[33,47,48] Elemental mapping of vertically aligned InGaN nanowires shows that growth begins with atomically registered InGaN and GaN domains that compete before the InGaN overtakes. The top of each nanowire is uniform, crystalline InGaN as confirmed by EDX (Figure 3E). Despite the reduced In content toward the substrate, a vertically continuous InGaN domain is commonly present throughout nanowires (Figure S4). Due to the size variations, the incorporation of indium is observed to be low at the nanowire bottom. Further optimization of the nanowire size and indium incorporation may lead to enhanced performance.

Pt nanoparticles as the co-catalyst for water reduction reaction have also been deposited on the InGaN nanowire surfaces, shown in Figure 3D, with a disperse distribution and a small size. In addition, small-size Pt nanoparticles (<10 nm) were deposited on InGaN nanowire surfaces, as shown in Figures 3D and 3G), to further accelerate water reduction reaction, wherein small-size photocatalyst performs better than bulk materials.[49–51] Moreover, its lattice spacing is determined to be ~2.3 Å along the [1$\bar{1}$1] direction, shown in Figure 3G, and contains facets and edges expected to behave as an efficient catalyst for proton reduction reaction (Figures S3 and S4).[50,51] In summary, such highly crystalline InGaN nanowires with small-size Pt nano-catalysts indicate the ability to perform efficient solar water-splitting

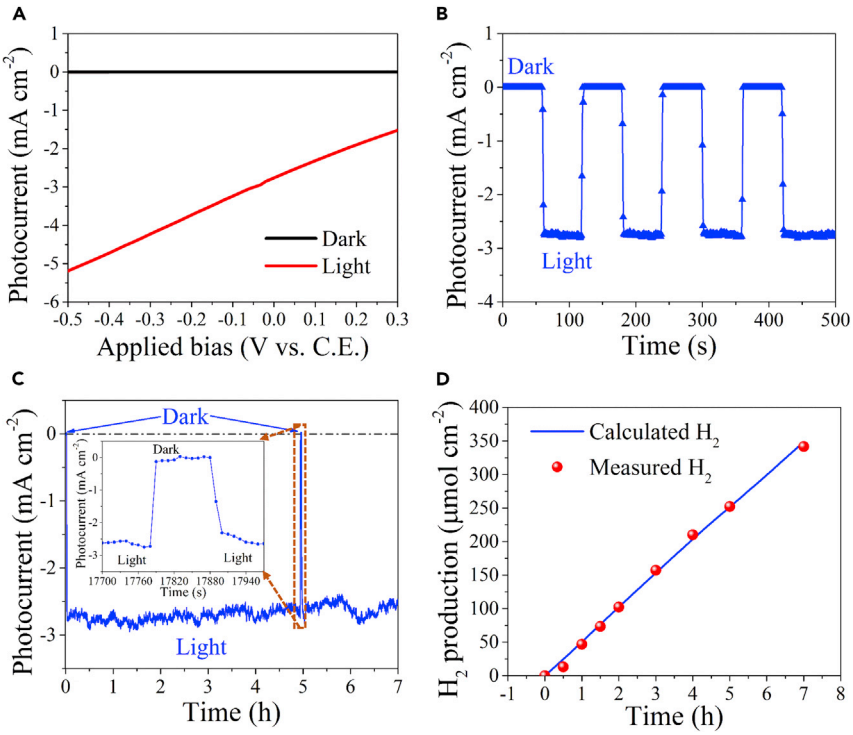

Figure 4. Unassisted Solar Water-Splitting Performance of $In_{0.25}Ga_{0.75}N$ Nanowire Photocathode in Two-Electrode Configuration versus Pt Counter Electrode

(A) Linear sweep voltammetry measurement under light and dark conditions.

(B) Variation of the photocurrent under cyclic light and dark conditions measured at zero bias versus Pt counter electrode.

(C) Continuous solar water-splitting experiment on $In_{0.25}Ga_{0.75}N$ nanowire tunnel-junction photocathode. The spikes correspond to brief dark current measurements, confirming that the observed current originates from light absorption of InGaN nanowires for solar hydrogen conversion.

(D) H_2 gas production (red dots) collected from (C) compared to the theoretical maximum value (blue curve) calculated from the electrons flowing through the circuit with a unity faradic efficiency. All the measurements were performed in 0.5 M H_2SO_4 solution under AM1.5G one-sun illumination, with a scanning rate of 20 mV/s.

application on $In_{0.25}Ga_{0.75}N$ nanowire photocathode. As shown in SEM and TEM images of such InGaN nanowires (Figures 2B, 3A, 3C, and S2), there is some non-uniformity in nanowire size, shape, and spacing that may limit the maximum achievable STH efficiency due to non-optimum light absorption, charge carrier extraction, dopant incorporation, and/or Pt co-catalyst deposition. Such issues can be potentially addressed by using the technique of selective area epitaxy to achieve uniform InGaN nanowire arrays.

Photoelectrochemical Performance of $In_{0.25}Ga_{0.75}N$ Nanowire Photocathode

Photoelectrochemical measurement of single-junction $In_{0.25}Ga_{0.75}N$ nanowire photocathode was performed in a dual-electrode configuration with a Pt counter electrode in 0.5 M H_2SO_4 acidic electrolyte solution under simulated AM1.5G one-sun illumination (see Experimental Procedures). It is important to note that the Pt electrode is not the best one for water oxidation reaction, which provides the opportunity to further improve the overall STH efficiency by adopting better optimized counter electrodes. Shown in Figure 4A is the LSV measurement of our best performing p-$In_{0.25}Ga_{0.75}N$ nanowire photocathode. In addition, the measured

dark current is negligible compared to the light current, suggesting that the measured photocurrent originates from solar energy conversion. This can be further confirmed under chopped light illumination, shown in Figure 4B, wherein dark and light cyclic photocurrent was continuously measured at zero bias versus counter electrode. A photocurrent of ~2.8 mA cm^{-2} is measured for $In_{0.25}Ga_{0.75}N$ nanowire photocathode at zero bias. Open circuit potential (OCP) measurement (data not shown) further suggests the downward surface band bending of p-type InGaN nanowires in electrolyte solution, which is well suited for electron extraction to drive proton reduction reaction.[52–55] Furthermore, the effect of using heavily doped silicon substrate is also studied (see Figure S5), which does not contribute to solar water splitting under light illumination but may lead to leakage current under negative biasing conditions. Additional LSV measurements were performed under light using 360 nm and 700 nm bandpass filters. There was no photocurrent measured under 700 nm light illumination at positive applied bias, whereas noticeable photocurrent was observed under 360 nm light illumination due to the PEC performance of p-InGaN nanowires (Figure S5B). At more negative bias, such heavily doped Si substrate could generate leakage current, if the Si surface is exposed to electrolyte solution.

Compared with previous work on III-nitride photoelectrodes,[22,26,27,56,57] the substantially improved onset potential and photocurrent density of the InGaN tunnel-junction nanowire photocathode is directly related to the efficient charge carrier separation, electron extraction, and hole collection enabled by the integration with InGaN tunnel junction. To achieve the best cathodic performance for unassisted solar water splitting, the growth conditions of $In_{0.25}Ga_{0.75}N$ nanowires were carefully optimized (see Experimental Procedures). It was identified that Mg doping incorporation played a critical role on the performance of InGaN nanowire photocathode (Figure S6). The best photoelectrode performance is achieved for InGaN nanowires using an Mg cell temperature of 210°C. Our recent studies have shown that the downward surface band bending of InGaN nanowires can be precisely engineered through controlled Mg dopant incorporation, which can enable efficient separation of photo-generated charge carriers.[31,32] It was also observed that surface treatment by HCl acid solution on InGaN nanowires can further enhance the performance significantly (Figure S7).

At zero bias, the STH efficiency is determined to be ~3.4%. Compared to the conventional three-electrode configuration with a reference electrode, the presented two-electrode measurements demonstrate unassisted solar water splitting performance.[14,16,17,27,58,59] The incident photon-to-current conversion efficiency (IPCE) of InGaN nanowire photocathode has been measured in two-electrode configuration at zero bias (Figure S8). We have further performed continuous, unassisted solar water-splitting measurements on such InGaN photocathodes (Figures 4C and 4D), where solar water-splitting photocurrent and H_2 gas production were measured at zero bias. The spikes in Figure 4C correspond to a brief dark current measurement, which was conducted intentionally to confirm the observed current originates from light absorption of InGaN nanowires for solar water splitting. Figure 4D shows the course of H_2 gas production (red dot) versus time, which is further compared with the theoretical value (solid blue line) calculated from the number of photo-generated electrons flowing through the circuit (see Supplemental Experimental Procedures). It is seen that the measured and calculated H_2 gas production, i.e., half of the photo-generated electron density, agree well, confirming a nearly unity faradic efficiency wherein all extracted photoexcited electrons drive solar water reduction reaction efficiently.[21,60]

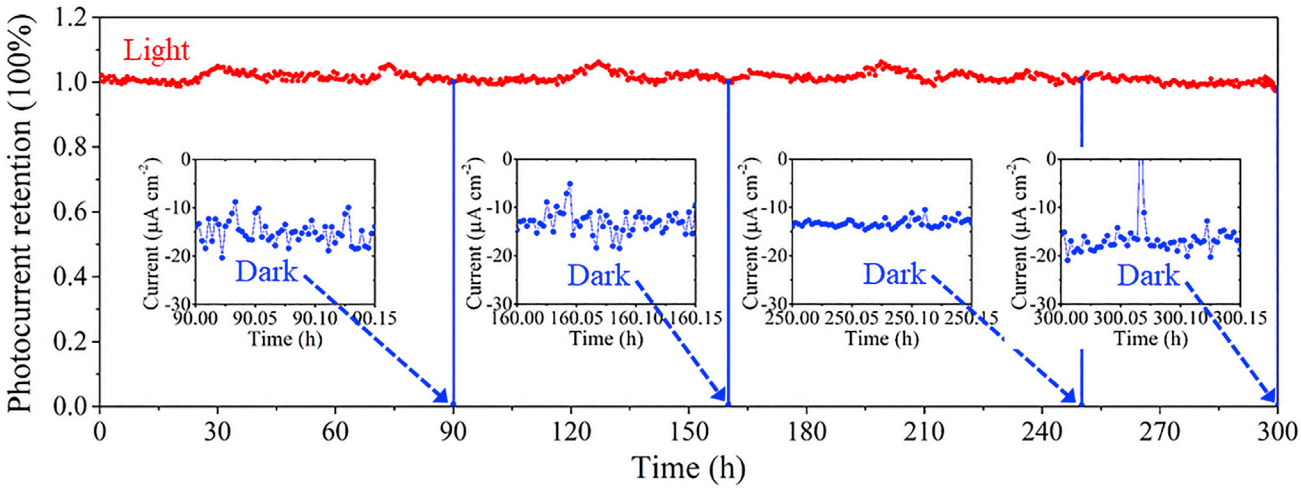

Figure 5. Long-Term Stability Evaluation of Single-Junction p-$In_{0.25}Ga_{0.75}N$ Nanowire Photocathode for Unassisted Solar Water Splitting

Photocurrent retention measured for ~300 h of unbiased solar water splitting versus Pt counter electrode. Brief dark current measurements were also shown after 90, 160, 250, and 300 h of stability testing, respectively. The measurement was performed in 0.5 M H_2SO_4 electrolyte solution under AM1.5G one-sun illumination.

Long-Term Stability for Unassisted Solar Water Splitting

Long-term stability evaluation of such $In_{0.25}Ga_{0.75}N$ nanowire photocathode for unassisted solar water splitting was further performed at 0 V versus Pt counter electrode in 0.5 M H_2SO_4 electrolyte solution under simulated one-sun illumination. Shown in Figure 5 is the measured photocurrent retention ratio over time. No significant performance degradation was observed for ~300 h, demonstrating excellent photoelectrochemical stability of InGaN nanowire photocathode. After 90, 160, 250, and 300 h stability test, the average measured dark currents (~15 μA cm^{-2}, ~13 μA cm^{-2}, ~13 μA cm^{-2}, and ~17 μA cm^{-2}, respectively) are negligible compared to the photocurrent, which suggests that the measured photocurrent originates from solar-to-hydrogen conversion during the stability testing. Moreover, another H_2 gas production was measured after stability testing, shown in Figure S9, which agrees well with the calculated values with a nearly unity faradic efficiency. Therefore, we can reasonably conclude that during the stability testing, the faradic efficiency is nearly unity wherein all the photocurrent drove H_2 gas production. For comparison, conventional Si and III-V photocathodes generally require the use of extra surface protection to achieve enhanced stability.[16,18,61] Structural properties of $In_{0.25}Ga_{0.75}N$ nanowires were characterized during the long-term stability measurements, and no obvious degradation was measured (Figure S10). After a long-term solar water-splitting experiment, a portion of Pt nanoparticles may be lost (Figure S11). The loss of some Pt co-catalysts may reduce the efficiency of charge carrier separation and proton reduction, which ultimately leads to degraded performance for the InGaN photocathode during solar water splitting. In addition, the underlying Si wafer may not be perfectly covered by Ga(In)N (Figure S12), which may also be a significant issue for long-term stability during solar water-splitting experiment.

DISCUSSION

Previously, InGaN materials have been studied for photocatalytic water splitting and HBr splitting.[21,23,26,31,32,57] In this work, we have demonstrated, for the first time, the use of InGaN photocathodes to achieve unassisted photoelectrochemical solar water splitting in a two-electrode configuration under AM1.5G one-sun illumination.

Photoelectrochemical performance of a single-junction $In_{0.25}Ga_{0.75}N$ nanowire photocathode is further compared with that of previously reported semiconductor photoelectrodes (Table S1). It is seen that high-efficiency photocathodes, using Z-scheme structures, are generally unstable, with stability limited to a few hours in two-electrode measurements, i.e., unassisted water-splitting experiments. Relatively long-term stable operation has been reported for photoelectrodes with the use of extra surface protection,[18,62] but these studies were generally performed in a three-electrode configuration, i.e., not unassisted water splitting. The measured stability of ~300 h for InGaN nanowire tunnel-junction photocathode stands out to be the best reported stability for single-junction photoelectrodes achieving unassisted photoelectrochemical solar water splitting (Table S1).

The realization of a single-junction InGaN photocathode with relatively high efficiency and long-term stability is attributed to the following factors: (1) high crystallinity and significantly reduced dislocations for nanowire structures grown directly on Si, (2) rapid separation of photo-generated charge carriers by optimizing the nanowire surface band bending through controlled Mg dopant incorporation, (3) efficient collection of photo-generated holes with the use of tunnel junction, (4) light trapping effect of the nanowire morphology for enhanced light absorption, and (5) N-terminated surfaces that can protect against photo-corrosion.[33,63] In addition, during epitaxy of InGaN nanowires, a thin (~20 nm) InGaN layer is also formed on the Si wafer, which can protect the InGaN-Si interface from photo-corrosion (Figure S12). Further improved performance is expected by replacing the Pt counter electrode with IrO_x or RuO_x electrodes to have more efficient water oxidation[22,64–69] and by optimizing the energy band gap of InGaN to enhance the photocurrent density. The device stability can also be improved by optimizing the deposition of co-catalysts.

In summary, we have demonstrated that a single-junction, InGaN nanowire photocathode integrated directly on Si wafer can drive relatively efficient and stable solar water splitting. An STH efficiency of 3.4% is measured at 0 V versus Pt counter electrode in 0.5 M H_2SO_4 electrolyte under AM1.5G one-sun illumination. The InGaN nanowire photocathode can operate relatively efficiently for ~300 h without additional passivation layers in unassisted solar water splitting. Significantly, such single-junction InGaN nanowire structures can be readily integrated with Si or GaAs bottom light absorbers to form a double-junction photoelectrode, which can potentially lead to STH > 20% with long-term stable operation. As shown in the SEM and TEM images (Figure 3), the InGaN nanowires look uniform overall but still have some variations in size and shape, which may limit the maximum STH. For example, light absorption on such InGaN nanowires may not be optimized. Charge carrier extraction may become less efficient if the nanowire size is too large and bulk recombination becomes dominant. In addition, the shadowing effect of nanowires may affect the uniformity of Mg doping and Pt co-catalyst deposition. These effects could limit the STH efficiency. In future work, such issues can be possibly addressed by using the special technique of selective area growth on patterned substrates, which can lead to the fabrication of uniform InGaN nanowire arrays. By further optimizing the epitaxy process and the size of nanowires, it is possible to minimize the formation of defects and dislocations due to the efficient surface strain relaxation.

EXPERIMENTAL PROCEDURES

Molecular Beam Epitaxial Growth of InGaN Nanowires

p-InGaN nanowire tunnel-junction structures were grown on n-type Si wafer (heavily doped, resistivity < 0.005 Ohm•cm) by plasma-assisted MBE in a nitrogen-rich

environment. The optimized growth parameters include a substrate temperature at 675°C, gallium (Ga) beam equivalent pressure (BEP) of 5E-8 Torr, indium (In) BEP of 6E-8 Torr, nitrogen flow rate of 1 sccm, and plasma power of 350 W. Firstly, n-type InGaN nanowire template was grown for 1 h using a germanium (Ge) source as the n-type dopant with a Ge cell temperature of 1,050°C. Then n^{++}/p^{++}-InGaN tunnel-junction nanostructure was integrated atop by growing 10 min n^{++}-InGaN doped by Ge at 1,080°C and 15 min p^{++}-InGaN using magnesium (Mg) with a Mg cell temperature of 290°C. Subsequently, a p-type InGaN segment with a Mg cell temperature of 210°C was grown to serve as the light absorber.

Deposition of Pt Co-catalyst Nanoparticles

Pt co-catalyst nanoparticles were deposited on InGaN nanowire surface by using a photodeposition method. In a vacuum-sealed chamber, the InGaN nanowire sample was immersed into a precursor solution including 55 mL deionized water, 11 mL methanol, and 10 μL 0.2 M H_2PtCl_6 solution. After pumping the chamber down for 10 min, InGaN nanowires were irradiated under 300 W xenon lamp through a quartz lid for 30 min. The sample was then rinsed in deionized water and dried using N_2 gas for subsequent photoelectrochemical measurements.

Photoelectrode Preparation

The platinized InGaN tunnel-junction nanowire integrated on Si wafer was further prepared as the photocathode for solar water-splitting measurements. A thin layer of In-Ga eutectic solution was first applied on backside of Si substrate forming metal contact, where a copper wire was connected using silver paste (Ted Pella, Fast Drying Silver Paint). The sample was then mounted to a glass slide using epoxy (Great Planes, 6-Minute Pro Epoxy), which sealed the sample back and edge with only InGaN nanowires exposed. The sample cured in air until stably mounted for any following measurement. It is important to minimize the surface area (<5%) covered by epoxy for measuring photoelectrode surface area accurately.

Photoelectrochemical Measurements

Photoelectrochemical measurements were conducted in a two-electrode configuration using a platinum counter electrode in 0.5 M H_2SO_4 electrolyte solution equipped with a solar simulator (Newport, LCS-100) with AM1.5G filter, which shows one-sun intensity. Light intensity of one sun was confirmed using a calibrated reference cell (Newport, 91150V). An electrochemical potentiostat instrument (Gamry, Interface 1010) was used to perform all the photoelectrochemical measurements, including linear sweep voltammetry, chronoamperometry, and OCP tests. The production of H_2 gas from solar water splitting on InGaN nanowires was analyzed by injecting 1 mL gas sampling into a gas chromatograph (Shimadzu, GC-8A). InGaN nanowire samples were treated in concentrated HCl acidic solution (Sigma-Aldrich) for 5 min before any photoelectrochemical measurement. The tested InGaN photocathodes have areal sizes in the range of 0.05~0.1 cm^2. For the three-electrode configuration, an additional Ag/AgCl reference electrode was used (in saturated KCl, $E_{(vs.\ RHE)} = +0.197\ V + E_{(vs.\ Ag/AgCl)} + 0.059 \times pH$ at 25°C).[34]

Structural and Optical Characterization

Photoluminescence spectroscopy of InGaN nanowires was performed using a He-Cd 325 nm excitation laser. SEM images were taken with a secondary electron (SE) detector using a Hitachi SU8000 system (5 kV), Tescan MIRA3 system (15 kV), and a JEOL IT500 SEM (10 kV) with an EDX detector. High-angle, annular dark-field scanning transmission electron microscopy (HAADF-STEM) images were collected using a JEOL 3100R05 microscope with Cs aberration corrected STEM (300 keV, 22 mrad)

with a camera length of 15 cm. The quantitative STEM-EDS analysis was performed using a JEOL 2100 probe-corrected STEM equipped with a horizontal ultra-thin window Si-Li X-ray detector (EDAX, active area ~30 mm^2). Samples for STEM characterization were prepared using bladed exfoliation or in cross-section view by mechanical wedge polishing.

SUPPLEMENTAL INFORMATION

Supplemental Information can be found online at https://doi.org/10.1016/j.joule.2019.07.022.

ACKNOWLEDGMENTS

This work was supported by the Office of Energy Efficiency and Renewable Energy, Fuel Cell Technologies Office under award no. EE0008086 and by the National Science Foundation under grant CBET 1804458. R.H. acknowledges support from the DOE Office of Science (DE-SC0011385). This work was performed in part at the University of Michigan Lurie Nanofabrication Facility. The authors acknowledge financial support from the University of Michigan College of Engineering and technical support from the Michigan Center for Materials Characterization.

AUTHOR CONTRIBUTIONS

Y.J.W. and Z.M. designed this study. Y.J.W. performed the MBE growth, PEC measurements, and material characterization. Y.P.W. contributed to PL measurement and TEM imaging. J.S., S.H.S., and R.H. conducted the electron microscope characterization. Y.J.W. and Z.M. analyzed the results and wrote the manuscript, with comments from all the authors.

DECLARATION OF INTERESTS

The authors declare no competing interests.

Received: April 14, 2019
Revised: June 2, 2019
Accepted: July 24, 2019
Published: August 22, 2019

REFERENCES

1. Walter, M.G., Warren, E.L., McKone, J.R., Boettcher, S.W., Mi, Q., Santori, E.A., and Lewis, N.S. (2010). Solar water splitting cells. Chem. Rev. *110*, 6446–6473.

2. Wang, S., Liu, G., and Wang, L. (2019). Crystal facet engineering of photoelectrodes for photoelectrochemical water splitting. Chem. Rev. *119*, 5192–5247.

3. Kuang, Y., Yamada, T., and Domen, K. (2017). Surface and interface engineering for photoelectrochemical water oxidation. Joule *1*, 290–305.

4. Gurudayal, Sabba, D., Kumar, M.H., Wong, L.H., Barber, J., Grätzel, M., and Mathews, N. (2015). Perovskite–hematite tandem cells for efficient overall solar driven water splitting. Nano Lett. *15*, 3833–3839.

5. Fujishima, A., and Honda, K. (1972). Electrochemical photolysis of water at a semiconductor electrode. Nature *238*, 37–38.

6. Cheng, W.-H., Richter, M.H., May, M.M., Ohlmann, J., Lackner, D., Dimroth, F., Hannappel, T., Atwater, H.A., and Lewerenz, H.-J. (2018). Monolithic photoelectrochemical device for direct water splitting with 19% efficiency. ACS Energy Lett. *3*, 1795–1800.

7. Verlage, E., Hu, S., Liu, R., Jones, R.J.R., Sun, K., Xiang, C., Lewis, N.S., and Atwater, H.A. (2015). A monolithically integrated, intrinsically safe, 10% efficient, solar-driven water-splitting system based on active, stable earth-abundant electrocatalysts in conjunction with tandem III-V light absorbers protected by amorphous TiO_2 films. Energy Environ. Sci. *8*, 3166–3172.

8. Shi, X., Zhang, K., Shin, K., Ma, M., Kwon, J., Choi, I.T., Kim, J.K., Kim, H.K., Wang, D.H., and Park, J.H. (2015). Unassisted photoelectrochemical water splitting beyond 5.7% solar-to-hydrogen conversion efficiency by a wireless monolithic photoanode/dye-sensitised solar cell tandem device. Nano Energy *13*, 182–191.

9. Martinez-Garcia, A., Russell, H.B., Paxton, W., Ravipati, S., Calero-Barney, S., Menon, M., Richter, E., Young, J., Deutsch, T., and Sunkara, M.K. (2018). Unassisted water splitting using a $GaSb_xP_{(1-x)}$ photoanode. Adv. Energy Mater. *8*, 1703247.

10. Khaselev, O., and Turner, J.A. (1998). A monolithic photovoltaic-photoelectrochemical device for dydrogen production via water splitting. Science *280*, 425–427.

11. Fountaine, K.T., Lewerenz, H.J., and Atwater, H.A. (2016). Efficiency limits for photoelectrochemical water-splitting. Nat. Commun. *7*, 13706.

12. Seger, B., Castelli, I.E., Vesborg, P.C.K., Jacobsen, K.W., Hansen, O., and Chorkendorff, I. (2014). 2-Photon tandem device for water splitting: comparing photocathode first versus photoanode first designs. Energy Environ. Sci. *7*, 2397–2413.

13. Kelly, N.A., and Gibson, T.L. (2006). Design and characterization of a robust photoelectrochemical device to generate hydrogen using solar water splitting. Int. J. Hydrog. Energy *31*, 1658–1673.

14. Reece, S.Y., Hamel, J.A., Sung, K., Jarvi, T.D., Esswein, A.J., Pijpers, J.J.H., and Nocera, D.G. (2011). Wireless solar water splitting using silicon-based semiconductors and earth-abundant catalysts. Science *334*, 645–648.

15. Gao, L., Cui, Y., Wang, J., Cavalli, A., Standing, A., Vu, T.T.T., Verheijen, M.A., Haverkort, J.E.M., Bakkers, E.P.A.M., and Notten, P.H.L. (2014). Photoelectrochemical hydrogen production on InP nanowire arrays with molybdenum sulfide electrocatalysts. Nano Lett. *14*, 3715–3719.

16. Fan, R., Huang, G., Wang, Y., Mi, Z., and Shen, M. (2018). Efficient n^+p-Si photocathodes for solar H_2 production catalyzed by Co-W-S and stabilized by Ti buffer layer. Appl. Catal. B *237*, 158–165.

17. Li, M., Luo, W., Cao, D., Zhao, X., Li, Z., Yu, T., and Zou, Z. (2013). A Co-catalyst-loaded Ta_3N_5 photoanode with a high solar photocurrent for water splitting upon facile removal of the surface layer. Angew. Chem. Int. Ed. *52*, 11016–11020.

18. Hu, S., Shaner, M.R., Beardslee, J.A., Lichterman, M., Brunschwig, B.S., and Lewis, N.S. (2014). Amorphous TiO_2 coatings stabilize Si, GaAs, and GaP photoanodes for efficient water oxidation. Science *344*, 1005–1009.

19. Shi, X., Jeong, H., Oh, S.J., Ma, M., Zhang, K., Kwon, J., Choi, I.T., Choi, I.Y., Kim, H.K., Kim, J.K., et al. (2016). Unassisted photoelectrochemical water splitting exceeding 7% solar-to-hydrogen conversion efficiency using photon recycling. Nat. Commun. *7*, 11943.

20. Young, J.L., Steiner, M.A., Döscher, H., France, R.M., Turner, J.A., and Deutsch, T.G. (2017). Direct solar-to-hydrogen conversion via inverted metamorphic multi-junction semiconductor architectures. Nat. Energy *2*, 17028.

21. AlOtaibi, B., Nguyen, H.P.T., Zhao, S., Kibria, M.G., Fan, S., and Mi, Z. (2013). Highly stable photoelectrochemical water splitting and hydrogen generation using a double-band InGaN/GaN core/shell nanowire photoanode. Nano Lett. *13*, 4356–4361.

22. Chu, S., Vanka, S., Wang, Y., Gim, J., Wang, Y., Ra, Y.-H., Hovden, R., Guo, H., Shih, I., and Mi, Z. (2018). Solar water oxidation by an InGaN nanowire photoanode with a bandgap of 1.7 eV. ACS Energy Lett. *3*, 307–314.

23. Guan, X., Chowdhury, F.A., Pant, N., Guo, L., Vayssieres, L., and Mi, Z. (2018). Efficient unassisted overall photocatalytic seawater splitting on GaN-based nanowire arrays. J. Phys. Chem. C *122*, 13797–13802.

24. Wang, D., Pierre, A., Kibria, M.G., Cui, K., Han, X., Bevan, K.H., Guo, H., Paradis, S., Hakima, A.R., and Mi, Z. (2011). Wafer-level photocatalytic water splitting on GaN nanowire arrays grown by molecular beam epitaxy. Nano Lett. *11*, 2353–2357.

25. Moses, P.G., and Van de Walle, C.G. (2010). Band bowing and band alignment in InGaN alloys. Appl. Phys. Lett. *96*, 021908.

26. Aryal, K., Pantha, B.N., Li, J., Lin, J.Y., and Jiang, H.X. (2010). Hydrogen generation by solar water splitting using p-InGaN photoelectrochemical cells. Appl. Phys. Lett. *96*, 052110.

27. Alvi, N.u.H., Soto Rodriguez, P.E.D., Aseev, P., Gómez, V.J., Alvi, A.u.H., Hassan, W.u., Willander, M., and Nötzel, R. (2015). InN/InGaN quantum dot photoelectrode: efficient hydrogen generation by water splitting at zero voltage. Nano Energy *13*, 291–297.

28. Sadaf, S.M., Ra, Y.H., Nguyen, H.P.T., Djavid, M., and Mi, Z. (2015). Alternating-current InGaN/GaN tunnel junction nanowire white-light emitting diodes. Nano Lett. *15*, 6696–6701.

29. Nguyen, H.P.T., Cui, K., Zhang, S., Djavid, M., Korinek, A., Botton, G.A., and Mi, Z. (2012). Controlling electron overflow in phosphor-free InGaN/GaN nanowire white light-emitting diodes. Nano Lett. *12*, 1317–1323.

30. Guo, W., Zhang, M., Banerjee, A., and Bhattacharya, P. (2010). Catalyst-free InGaN/GaN nanowire light emitting diodes grown on (001) silicon by molecular beam epitaxy. Nano Lett. *10*, 3355–3359.

31. Chowdhury, F.A., Trudeau, M.L., Guo, H., and Mi, Z. (2018). A photochemical diode artificial photosynthesis system for unassisted high efficiency overall pure water splitting. Nat. Commun. *9*, 1707.

32. Kibria, M.G., Zhao, S., Chowdhury, F.A., Wang, Q., Nguyen, H.P.T., Trudeau, M.L., Guo, H., and Mi, Z. (2014). Tuning the surface Fermi level on p-type gallium nitride nanowires for efficient overall water splitting. Nat. Commun. *5*, 3825.

33. Kibria, M.G., Qiao, R., Yang, W., Boukahil, I., Kong, X., Chowdhury, F.A., Trudeau, M.L., Ji, W., Guo, H., Himpsel, F.J., et al. (2016). Atomic-scale origin of long-term stability and high performance of p-GaN nanowire arrays for photocatalytic overall pure water splitting. Adv. Mater. *28*, 8388–8397.

34. Vanka, S., Arca, E., Cheng, S., Sun, K., Botton, G.A., Teeter, G., and Mi, Z. (2018). High efficiency Si photocathode protected by multifunctional GaN nanostructures. Nano Lett. *18*, 6530–6537.

35. Wang, Q., Hisatomi, T., Suzuki, Y., Pan, Z., Seo, J., Katayama, M., Minegishi, T., Nishiyama, H., Takata, T., Seki, K., et al. (2017). Particulate photocatalyst sheets based on carbon conductor layer for efficient Z-scheme pure-water splitting at ambient pressure. J. Am. Chem. Soc. *139*, 1675–1683.

36. Sadaf, S.M., Zhao, S., Wu, Y., Ra, Y.H., Liu, X., Vanka, S., and Mi, Z. (2017). An AlGaN core-shell tunnel junction nanowire light-emitting diode operating in the ultraviolet-C band. Nano Lett. *17*, 1212–1218.

37. Ebaid, M., Min, J.-W., Zhao, C., Ng, T.K., Idriss, H., and Ooi, B.S. (2018). Water splitting to hydrogen over epitaxially grown InGaN nanowires on a metallic titanium/silicon template: reduced interfacial transfer resistance and improved stability to hydrogen. J. Mater. Chem. A *6*, 6922–6930.

38. Liu, C., Tang, J., Chen, H.M., Liu, B., and Yang, P. (2013). A fully integrated nanosystem of semiconductor nanowires for direct solar water splitting. Nano Lett. *13*, 2989–2992.

39. Jiang, Z., Zhang, Z., Shangguan, W., Isaacs, M.A., Durndell, L.J., Parlett, C.M.A., and Lee, A.F. (2016). Photodeposition as a facile route to tunable Pt photocatalysts for hydrogen production: on the role of methanol. Catal. Sci. Technol. *6*, 81–88.

40. Cheng, N., Stambula, S., Wang, D., Banis, M.N., Liu, J., Riese, A., Xiao, B., Li, R., Sham, T.K., Liu, L.M., et al. (2016). Platinum single-atom and cluster catalysis of the hydrogen evolution reaction. Nat. Commun. *7*, 13638.

41. Kibria, M.G., Chowdhury, F.A., Zhao, S., AlOtaibi, B., Trudeau, M.L., Guo, H., and Mi, Z. (2015). Visible light-driven efficient overall water splitting using p-type metal-nitride nanowire arrays. Nat. Commun. *6*, 6797.

42. Benton, J., Bai, J., and Wang, T. (2014). Utilisation of GaN and InGaN/GaN with nanoporous structures for water splitting. Appl. Phys. Lett. *105*, 223902.

43. Ebaid, M., Kang, J.H., Yoo, Y.S., Lim, S.H., Cho, Y.H., and Ryu, S.W. (2015). Vertically aligned InGaN nanowires with engineered axial In composition for highly efficient visible light emission. Sci. Rep. *5*, 17003.

44. Goodman, K.D., Protasenko, V.V., Verma, J., Kosel, T.H., Xing, H.G., and Jena, D. (2011). Green luminescence of InGaN nanowires grown on silicon substrates by molecular beam epitaxy. J. Appl. Phys. *109*, 084336.

45. Krishna, T.C.S., and Gupta, G. (2014). Band alignment and Schottky behaviour of InN/GaN heterostructure grown by low-temperature low-energy nitrogen ion bombardment. RSC Adv *4*, 27308–27314.

46. Kibria, M.G., and Mi, Z. (2016). Artificial photosynthesis using metal/nonmetal-nitride semiconductors: current status, prospects, and challenges. J. Mater. Chem. A *4*, 2801–2820.

47. Komaki, H., Katayama, R., Onabe, K., Ozeki, M., and Ikari, T. (2007). Nitrogen supply rate dependence of InGaN growth properties, by RF-MBE. J. Cryst. Growth *305*, 12–18.

48. Duff, A.I., Lymperakis, L., and Neugebauer, J. (2015). Ab initio-based bulk and surface thermodynamics of InGaN alloys: investigating the effects of strain and surface polarity. Phys. Status Solidi B *252*, 855–865.

49. Tan, T.L., Wang, L.-L., Zhang, J., Johnson, D.D., and Bai, K. (2015). Platinum nanoparticle during electrochemical hydrogen evolution: adsorbate distribution, active reaction species, and size effect. ACS Catal *5*, 2376–2383.

50. Wei, G.F., and Liu, Z.P. (2015). Restructuring and hydrogen evolution on Pt nanoparticle. Chem. Sci. *6*, 1485–1490.

51. Zalitis, C.M., Kucernak, A.R., Sharman, J., and Wright, E. (2017). Design principles for platinum nanoparticles catalysing electrochemical hydrogen evolution and oxidation reactions: edges are much more active than facets. J. Mater. Chem. A *5*, 23328–23338.

52. Berglund, S.P., Abdi, F.F., Bogdanoff, P., Chemseddine, A., Friedrich, D., and van de Krol, R. (2016). Comprehensive evaluation of $CuBi_2O_4$ as a photocathode material for photoelectrochemical water splitting. Chem. Mater *28*, 4231–4242.

53. Das, C., Tallarida, M., and Schmeisser, D. (2015). Si microstructures laminated with a nanolayer of TiO_2 as long-term stable and effective photocathodes in PEC devices. Nanoscale *7*, 7726–7733.

54. Jung, J.Y., Yu, J.Y., and Lee, J.H. (2018). Dynamic photoelectrochemical device using an electrolyte-permeable NiO_x/SiO_2/Si photocathode with an open-circuit potential of 0.75 V. ACS Appl. Mater. Interfaces *10*, 7955–7962.

55. ElAfandy, R.T., Ebaid, M., Min, J.W., Zhao, C., Ng, T.K., and Ooi, B.S. (2018). Flexible InGaN nanowire membranes for enhanced solar water splitting. Opt. Express *26*, A640–A650.

56. Luo, W., Liu, B., Li, Z., Xie, Z., Chen, D., Zou, Z., and Zhang, R. (2008). Stable response to visible light of InGaN photoelectrodes. Appl. Phys. Lett. *92*, 262110.

57. Hwang, Y.J., Wu, C.H., Hahn, C., Jeong, H.E., and Yang, P. (2012). Si/InGaN core/shell hierarchical nanowire arrays and their photoelectrochemical properties. Nano Lett. *12*, 1678–1682.

58. Weng, B., Grice, C.R., Ge, J., Poudel, T., Deng, X., and Yan, Y. (2018). Barium bismuth niobate double perovskite/tungsten oxide nanosheet photoanode for high-performance photoelectrochemical water splitting. Adv. Energy Mater. *8*, 1701655.

59. Zhao, Y., Yang, K.R., Wang, Z., Yan, X., Cao, S., Ye, Y., Dong, Q., Zhang, X., Thorne, J.E., Jin, L., et al. (2018). Stable iridium dinuclear heterogeneous catalysts supported on metal-oxide substrate for solar water oxidation. Proc. Natl. Acad. Sci. USA *115*, 2902–2907.

60. Svengren, H., Chamoun, M., Grins, J., and Johnsson, M. (2018). Water splitting catalysis studied by using real-time Faradaic efficiency obtained through coupled electrolysis and mass spectrometry. ChemElectroChem *5*, 44–50.

61. Liu, R., Zheng, Z., Spurgeon, J., and Yang, X. (2014). Enhanced photoelectrochemical water-splitting performance of semiconductors by surface passivation layers. Energy Environ. Sci. *7*, 2504–2517.

62. Shaner, M.R., Hu, S., Sun, K., and Lewis, N.S. (2015). Stabilization of Si microwire arrays for solar-driven H_2O oxidation to O_2(g) in 1.0 M KOH(aq) using conformal coatings of amorphous TiO_2. Energy Environ. Sci. *8*, 203–207.

63. Zhou, B., Kong, X., Vanka, S., Chu, S., Ghamari, P., Wang, Y., Pant, N., Shih, I., Guo, H., and Mi, Z. (2018). Gallium nitride nanowire as a linker of molybdenum sulfides and silicon for photoelectrocatalytic water splitting. Nat. Commun. *9*, 3856.

64. Roger, I., Shipman, M.A., and Symes, M.D. (2017). Earth-abundant catalysts for electrochemical and photoelectrochemical water splitting. Nat. Rev. Chem. *1*, 0003.

65. Shi, X., Siahrostami, S., Li, G.L., Zhang, Y., Chakthranont, P., Studt, F., Jaramillo, T.F., Zheng, X., and Nørskov, J.K. (2017). Understanding activity trends in electrochemical water oxidation to form hydrogen peroxide. Nat. Commun. *8*, 701.

66. Rui, K., Zhao, G., Chen, Y., Lin, Y., Zhou, Q., Chen, J., Zhu, J., Sun, W., Huang, W., and Dou, S.X. (2018). Hybrid 2D dual-metal–organic frameworks for enhanced water oxidation catalysis. Adv. Funct. Mater. *28*, 1801554.

67. Wang, Y., Zhao, S., Wang, Y., Laleyan, D.A., Wu, Y., Ouyang, B., Ou, P., Song, J., and Mi, Z. (2018). Wafer-scale synthesis of monolayer WSe_2: a multi-functional photocatalyst for efficient overall pure water splitting. Nano Energy *51*, 54–60.

68. Zhang, P., Li, L., Nordlund, D., Chen, H., Fan, L., Zhang, B., Sheng, X., Daniel, Q., and Sun, L. (2018). Dendritic core-shell nickel-iron-copper metal/metal oxide electrode for efficient electrocatalytic water oxidation. Nat. Commun. *9*, 381.

69. Zheng, M., Ding, Y., Cao, X., Tian, T., and Lin, J. (2018). Homogeneous and heterogeneous photocatalytic water oxidation by polyoxometalates containing the most earth-abundant transition metal, iron. Appl. Catal. B *237*, 1091–1100.